IAC-16-C1.9.2

Orbit-Attitude Coupled Motion Around Small Bodies: Sun-Synchronous Orbits with Sun-Tracking Attitude Motion

Shota Kikuchi[a]*, Kathleen C. Howell[b], Yuichi Tsuda[c], and Jun'ichiro Kawaguchi[d]

[a] *Department of Aeronautics and Astronautics, The University of Tokyo, 7-3-1 Hongo, Bunkyo-ku, Tokyo, Japan, 113-0033,* kikuchi.shota@ac.jaxa.jp
[b] *School of Aeronautics and Astronautics, Purdue University, 701 West Stadium Avenue, West Lafayette, IN 47906*, howell@purdue.edu
[c] *Institute of Space and Astronautical Science, Japan Aerospace Exploration Agency, 3-1-1 Yoshinodai, Chuo-ku, Sagamihara, Kanagawa, Japan 252-0222*, tsuda.yuichi@jaxa.jp
[d] *Institute of Space and Astronautical Science, Japan Aerospace Exploration Agency, 3-1-1 Yoshinodai, Chuo-ku, Sagamihara, Kanagawa, Japan 252-0222*, kawaguchi.junichiro@jaxa.jp
* Corresponding Author

Abstract

The motion of a spacecraft in the proximity of a small body is significantly perturbed primarily due to the irregular shape of the small body and solar radiation pressure. In such a strongly perturbed environment, the coupling effect of the orbital and attitude motions has a large effect that cannot be neglected. However, natural orbit-attitude coupled dynamics around small bodies that are stationary in both orbital and attitude motions have yet to be observed. The present study therefore investigates natural coupled motion that involves both a Sun-synchronous orbit and Sun-tracking attitude motion. This orbit-attitude coupled motion enables a spacecraft to maintain its orbital geometry and attitude state with respect to the Sun without requiring active control. The proposed method can reduce the use of an orbit and attitude control system, which reduces the weight of a spacecraft and prolongs the life time of the mission. This study provides evidence that Sun-synchronous orbits with Sun-tracking attitude motion are feasible for small-body missions and exhibit unique dynamic characteristics.

Keywords: Small body, Solar radiation pressure, Gravity irregularity, Sun-synchronous orbit, Sun-tracking motion, Orbit-attitude coupled motion

1. Introduction

Rendezvous missions to small bodies, such as asteroids and comets, have been of interest in recent years. In such missions, the motion of a spacecraft around a small body is strongly perturbed primarily due to the irregular gravity field and solar radiation pressure (SRP). These perturbations significantly influence both the orbital and attitude motions of the spacecraft; thus, the dynamical environment around a small body completely differs from those around planets and moons. To understand this unique environment, many previous studies have analyzed orbital and attitude dynamics around small bodies.

With regard to orbital motion around a small body, gravity irregularity due to the oblateness of the body and the SRP perturbation are the two predominant perturbing forces, which can lead to significant changes in orbital elements [1]. One of the classical approaches to this problem is implementing Sun-synchronous frozen orbits, for which the orbital geometries are constant with respect to the Sun, as depicted in Fig. 1 (left). Previous studies have revealed that Sun-synchronous orbits can be achieved when either or both the oblateness effect and SRP perturbation are dominant [2 – 5]. Therefore, Sun-synchronous orbits are useful options for small-body missions.

On the other hand, with regard to attitude motion around a small body, most published studies focused on the effect of higher-order gravity gradient (GG) torque acting on a spacecraft as a result of gravity irregularity. The attitude dynamics of a spacecraft subject to this effect have been formulated and analyzed [6, 7], and the attitude motion has been found to be affected by the shape of the small body [8]. In addition to GG torque, the torque due to SRP can also disturb the attitude of a spacecraft, depending on the system [9]. For these reasons, the attitude motion of a spacecraft around a small body is strongly perturbed, resulting in complex dynamics.

In the studies described above, the orbital motion and the attitude motion of a spacecraft have been analyzed independently, by assuming constant attitude states or stationary circular orbits. However, these motions are not independent in reality, such that there is a dynamic interaction between them. For example, the gravitational force and the SRP force are dependent on the attitude of a spacecraft when the spacecraft is modelled as a rigid body [10]. On the other hand, GG torque is dependent on the position of a spacecraft with

respect to a gravitational mass. With regard to multi-body dynamics, past studies have analyzed the effects of GG torque and SRP torque on libration point orbits in the interplanetary region [11, 12]. Within the same regime, further investigation has identified periodic solutions of such orbit-attitude coupled motion [13].

Recent studies have revealed that such orbit-attitude coupling effect also significantly impacts the motion of a spacecraft around a small body [14 - 16]. It has therefore been concluded that modelling the motion of a spacecraft around a small body as orbit-attitude coupled dynamics is necessary for precise analyses. However, natural coupled dynamics that are stationary in both orbital and attitude motions have yet to be identified. Moreover, past studies regarding attitude motion around small bodies have evaluated the attitude of a spacecraft with respect to a small body [6, 8, 15], although attitude motion with respect to the Sun can also significantly affect real missions.

Therefore, the present study investigates natural orbit-attitude coupled motion that involves both a Sun-synchronous orbit and a Sun-tracking attitude motion, as depicted in Fig. 1. Sun-tracking attitude motion is the natural motion, by which the specific axis of a spacecraft continuously tracks the direction of the Sun, as implemented in the Hayabusa and Hayabusa 2 mission in the interplanetary region [17, 18]. The proposed orbit-attitude coupled motion around a small body enables a spacecraft to maintain its orbital geometry and attitude state with respect to the Sun without requiring any active control. Thus, the proposed method is advantageous for solar power generation, thermal design, and optical observation. Moreover, it can reduce the use of orbit and attitude control systems, such as thrusters and reaction wheels, thereby reducing the weight of a spacecraft, prolonging the life time of the mission, and reducing the operational workload.

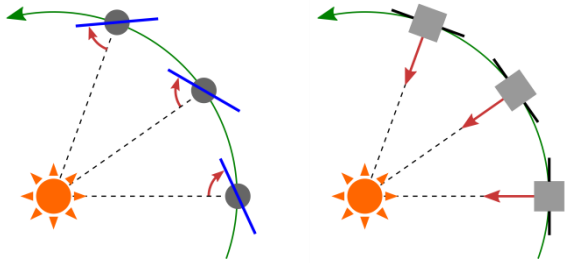

Fig. 1. Sun-synchronous orbit (left) and Sun-tracking attitude motion (right)

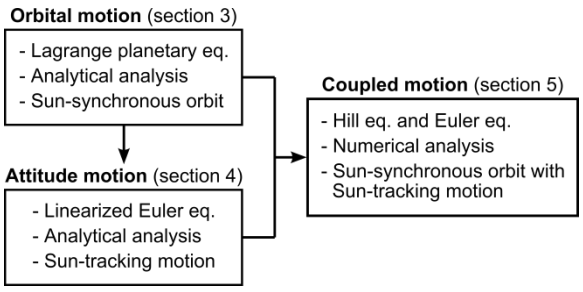

Fig. 2. Research process

The present study was designed to develop general theories behind achieving Sun-synchronous orbits with Sun-tracking attitude motions around small bodies and to verify the feasibility of such motions. Toward this end, this paper is composed of three parts, as shown in Fig. 2. First, the orbital motion is modelled as Lagrange planetary equations, and the solutions of Sun-synchronous orbits are solved. Second, the attitude motion is modelled as linearized Euler equations, considering the Sun-synchronous orbits obtained in the first step, and conditions required to achieve Sun-tracking motion are derived. Finally, the orbital and attitude motions are propagated by numerical integration, based on coupled orbit-attitude equations of motion. Ultimately, it is demonstrated that a Sun-synchronous orbit with Sun-tracking attitude motion can be achieved via an orbit-attitude coupled system around a small body.

2. Dynamic model

2.1 Spacecraft and small body model

The physical parameters for a spacecraft used in this paper are given in Table 1. Although these parameters are based on the Hayabusa 2 spacecraft [18, 19], which was launched by JAXA in 2014, it is assumed that the spacecraft has an axisymmetrical shape for simplicity. Throughout this paper, the z axis of the spacecraft body-fixed frame is regarded as the axis that should be directed toward the direction of the Sun, that is, the normal direction of solar array panels, for example. C_s, C_d, and C_a are optical constants of the spacecraft surface that correspond to the modes of specular reflection, diffuse reflection, and absorption, respectively, which satisfy $C_s + C_d + C_a = 1$.

Table 1. Spacecraft parameters

Item	Symbol	Value
Mass	m	600 kg
Area	A	13 m^2
Moments of Inertia	I_x, I_y, I_z	360, 360, 480 kg · m^2
CS-CM distance*	L	0.2 m
Optical constants	C_s, C_d, C_a	0.1, 0.1, 0.8

CS: Center of SRP; CM: Center of mass

Table 2. Small body parameters

Item	Symbol	Value
Distance from the Sun	d	1 AU
Mean diameter		1 km
Axis ratio	$R_a : R_b : R_c$	1.4: 1.2: 1
Density		2.6 g/cm^3
Rotation period	T_{rot}	7 hr

The physical parameters for a small body are given in Table 2. The body is assumed to be moving in a circular orbit, with a radius of 1 AU, around the Sun. The body is modelled as a homogeneous triaxial ellipsoid, with a mean diameter of 1 km, rotating uniformly about the shortest axis. This rotation axis is assumed to be perpendicular to the ecliptic plane. The rotation axis can take any direction in general; however, near Earth asteroids and main belt asteroids with small diameters ($\lesssim$ 30 km) show a lack of rotation axes close to the ecliptic plane [5, 20]. Therefore, this assumption regarding the rotation axis is reasonable for initial analyses. The bulk density of the body is assumed to be the same as the common value of a C-type asteroid [21].

2.2. Coordinate system

2.2.1 Definitions of coordinate systems

To describe the orbital and attitude motions of a spacecraft, six different coordinate systems are used, as shown in Fig. 3.

- Inertial coordinate: (x^I, y^I, z^I)

The origin is at the center of the Sun. All axes are fixed in the inertial space.

- Hill coordinate: (x^H, y^H, z^H)

The origin is at the center of a small body. The x axis points in the anti-Sun direction, the z axis is aligned with the angular velocity vector of the orbit of the small body around the Sun, and the y axis completes a right-handed Cartesian coordinate system.

- Small-body-fixed coordinate: (x^{SB}, y^{SB}, z^{SB})

The x, y, and z axes are fixed on the longest, intermediate, and shortest axis, respectively, of the small body. The z axis is identical to z^H because of the assumption given in the previous subsection.

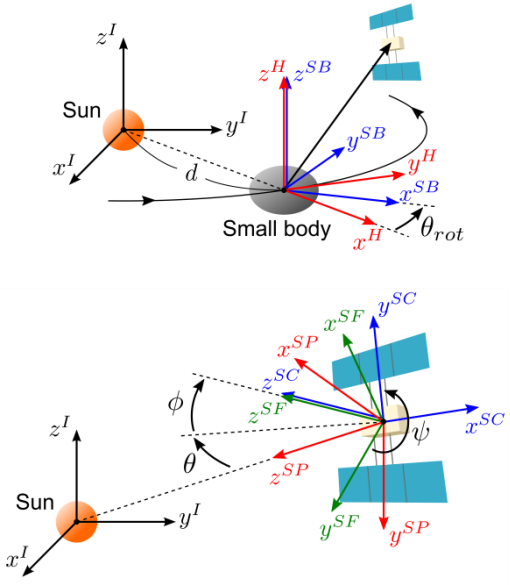

Fig. 3. Coordinate systems

- Sun-pointing coordinate: (x^{SP}, y^{SP}, z^{SP})

The origin is at the center of the spacecraft. The z axis points in the Sun direction, the x axis is perpendicular to the plane formed by x^H and y^H, and the y axis completes a right-handed Cartesian coordinate system.

- Spin-free coordinate: (x^{SF}, y^{SF}, z^{SF})

The origin is at the center of the spacecraft. The z axis is fixed on the spacecraft, the x axis is perpendicular to the plane formed by x^{SP} and y^{SP}, and the y axis completes a right-handed Cartesian coordinate system.

- Spacecraft-fixed coordinate: (x^{SC}, y^{SC}, z^{SC})

The origin is at the center of the spacecraft. All axes are fixed on the spacecraft and are aligned along the principal directions. The z axis is identical to z^{SF}.

From these definitions, the attitude of the spacecraft can be expressed by Euler angles (ϕ, θ, ψ), considering a 2-1-3 rotation sequence from the Sun-pointing coordinate to the spacecraft-fixed coordinate. Because the distance between the small body and the spacecraft is sufficiently smaller than that between the Sun and the small body, θ and ϕ can be regarded as in-plane and out-of-plane Sun angles with respect to the ecliptic plane.

2.1.2 Transformations between coordinate systems

Let ${}^{\xi}\boldsymbol{u}$ denote a 3-dimensional vector in an arbitrary ξ-coordinate system, and let ${}^{\eta}\boldsymbol{C}_{\xi}$ denote the rotational transformation matrix from an ξ-coordinate to an η-coordinate system. Then, the rotational coordinate transformation for the vector is expressed as ${}^{\eta}\boldsymbol{u} = {}^{\eta}\boldsymbol{C}_{\xi}{}^{\xi}\boldsymbol{u}$. The rotational coordinate transformation matrices between some of the coordinate systems are given in the following part. Here, the rotational transformation matrices about the x, y, and z axes by an angle ϑ are denoted as $\boldsymbol{R}_x(\vartheta)$, $\boldsymbol{R}_y(\vartheta)$, and $\boldsymbol{R}_z(\vartheta)$.

When the rotation angle of a small body with respect to the Hill coordinate is denoted by θ_{rot}, as shown in Fig. 3, the rotational transformation from the Hill coordinate to the small-body-fixed coordinate is given by the equation below.

$$ {}^{SB}\boldsymbol{C}_H = \boldsymbol{R}_z(\theta_{rot}) \tag{1}$$

Let θ_1 and θ_2 be defined as

$$ \theta_1 = \tan^{-1}\frac{y}{d+x}, \quad \theta_2 = \tan^{-1}\frac{z}{d+x} \tag{2}$$

where (x, y, z) denotes the position of the spacecraft in terms of the Hill coordinate. Because $x, y, z \ll d$ holds in the proximity of a small body, the rotational transformation from the Hill coordinate to the Sun-pointing coordinate is given by the following equation:

$$
\begin{aligned}
{}^{SP}\boldsymbol{C}_H &= \boldsymbol{R}_x(-\theta_2)\boldsymbol{R}_y(-\theta_1)\boldsymbol{R}_x\left(-\frac{\pi}{2}\right)\boldsymbol{R}_z\left(\frac{\pi}{2}\right) \\
&\simeq \boldsymbol{R}_x\left(-\frac{\pi}{2}\right)\boldsymbol{R}_z\left(\frac{\pi}{2}\right)
\end{aligned} \tag{3}
$$

Considering a 2-1-3 rotation sequence with a rotation angle set of $(\phi, \theta, 0)$, the rotational transformation from the Sun-pointing coordinate to the spin-free coordinate is expressed as follows:

$$
{}^{SF}\boldsymbol{C}_{SP} = \boldsymbol{R}_x(\phi)\boldsymbol{R}_y(\theta) \tag{4}
$$

Considering a 2-1-3 rotation sequence with a rotation angle set of (ϕ, θ, ψ), the rotational transformation from the Sun-pointing coordinate to the spacecraft-fixed coordinate is expressed as follows:

$$
{}^{SC}\boldsymbol{C}_{SP} = \boldsymbol{R}_z(\psi)\boldsymbol{R}_x(\phi)\boldsymbol{R}_y(\theta) = \boldsymbol{R}_z(\psi)\,{}^{SF}\boldsymbol{C}_{SP} \tag{5}
$$

2.3 Gravity model

The gravity of a small body is calculated based on an ellipsoid model. The gravitational coefficients C_{mn} of its spherical harmonics expansion up to the fourth order are defined by Eq. (56) in the Appendix. Using these coefficients, the gravitational potential of a mass element due to the zeroth-, second-, and fourth-order gravity terms can be expressed as follows [7, 24]:

$$
\begin{aligned}
U_{G,C_{00}} &= \frac{\mu}{|\boldsymbol{R}|} \\
U_{G,C_{2k}} &= \mu C_{20} R_a^2 \left(\frac{3}{2}\frac{(\boldsymbol{\gamma}\cdot\boldsymbol{R})^2}{|\boldsymbol{R}|^5} - \frac{1}{2}\frac{1}{|\boldsymbol{R}|^3} \right) \\
&\quad + \mu C_{22} R_a^2 \cdot 3 \frac{(\boldsymbol{\alpha}\cdot\boldsymbol{R})^2 - (\boldsymbol{\beta}\cdot\boldsymbol{R})^2}{|\boldsymbol{R}|^5} \\
U_{G,C_{4k}} &= \mu C_{40} R_a^4 \left(\frac{35}{8}\frac{(\boldsymbol{\gamma}\cdot\boldsymbol{R})^4}{|\boldsymbol{R}|^9} - \frac{15}{4}\frac{(\boldsymbol{\gamma}\cdot\boldsymbol{R})^2}{|\boldsymbol{R}|^7} + \frac{3}{8}\frac{1}{|\boldsymbol{R}|^5} \right) \\
&\quad + \mu C_{42} R_a^4 \left(\frac{105}{2}\frac{\{(\boldsymbol{\alpha}\cdot\boldsymbol{R})^2 - (\boldsymbol{\beta}\cdot\boldsymbol{R})^2\}(\boldsymbol{\gamma}\cdot\boldsymbol{R})^2}{|\boldsymbol{R}|^9} \right. \\
&\quad \left. - \frac{15}{2}\frac{(\boldsymbol{\alpha}\cdot\boldsymbol{R})^2 - (\boldsymbol{\beta}\cdot\boldsymbol{R})^2}{|\boldsymbol{R}|^7} \right) \\
&\quad + \mu C_{44} R_a^4 \left(105\frac{(\boldsymbol{\alpha}\cdot\boldsymbol{R})^4 + (\boldsymbol{\beta}\cdot\boldsymbol{R})^4}{|\boldsymbol{R}|^9} \right. \\
&\quad \left. - 630\frac{(\boldsymbol{\alpha}\cdot\boldsymbol{R})^2(\boldsymbol{\beta}\cdot\boldsymbol{R})^2}{|\boldsymbol{R}|^9} \right)
\end{aligned} \tag{6}
$$

Here, $\boldsymbol{\alpha}$, $\boldsymbol{\beta}$, and $\boldsymbol{\gamma}$ denote unit vectors along the longest, intermediate, and shortest axes of the small body, respectively, and $\boldsymbol{R}$ denotes the relative position vector of a mass element with respect to the center of mass of the small body, as shown in Fig. 4. $\boldsymbol{R}$ can be expressed as follows:

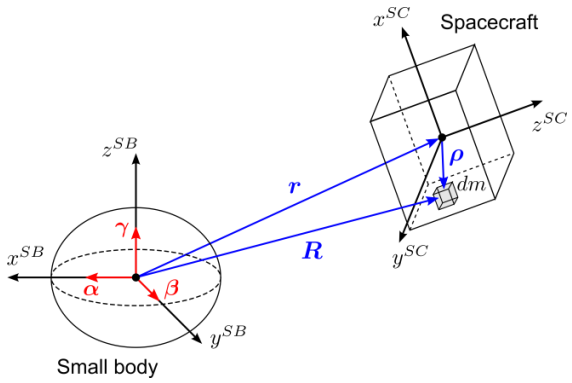

Fig. 4. Position of a spacecraft relative to a small body

$$
\boldsymbol{R} = \boldsymbol{r} + \boldsymbol{\rho} \tag{7}
$$

where $\boldsymbol{r}$ is the relative position vector of the center of mass of the spacecraft relative to that of the small body, and $\boldsymbol{\rho}$ is the relative position vector of the element relative to the center of mass of the spacecraft.

Considering the derivative of the gravitational potentials with respect to $\boldsymbol{R}$, the gravitational force and the GG torque can be expressed by Eqs. (8) and (9).

$$
\begin{aligned}
\boldsymbol{F}_G &= \int \frac{\partial U_{G,C_{00}}}{\partial \boldsymbol{R}} dm + m\frac{\partial U_{G,C_{2k}}}{\partial \boldsymbol{R}}\bigg|_{\boldsymbol{R}=\boldsymbol{r}} + m\frac{\partial U_{G,C_{4k}}}{\partial \boldsymbol{R}}\bigg|_{\boldsymbol{R}=\boldsymbol{r}} \\
&\equiv \boldsymbol{F}_{G,C_{00}} + \boldsymbol{F}_{G,coup} + \boldsymbol{F}_{G,C_{2k}} + \boldsymbol{F}_{G,C_{4k}}
\end{aligned} \tag{8}
$$

$$
\begin{aligned}
\boldsymbol{T}_{GG} &= \int \boldsymbol{\rho} \times \frac{\partial U_{G,C_{00}}}{\partial \boldsymbol{R}} dm + \int \boldsymbol{\rho} \times \frac{\partial U_{G,C_{2m}}}{\partial \boldsymbol{R}} dm \\
&\equiv \boldsymbol{T}_{GG,C_{00}} + \boldsymbol{T}_{GG,C_{2k}}
\end{aligned} \tag{9}
$$

These equations assume that the gravitational potential up to the fourth order contributes to the force acting on the spacecraft, while the potential up to the second order contributes to the torque. In Eq. (8), the spacecraft is treated as a point mass for the calculation of the gravitational force due to the second- and fourth-order terms. By contrast, the shape of the spacecraft is taken into account for the force due to the zeroth-order term, which means that the attitude of the spacecraft exerts influence on the orbital motion, thereby causing the gravitational coupling effect [14, 16]. The explicit formulations of the terms described in Eqs. (8) and (9) are provided by Eqs. (60) and (61) in the Appendix.

2.4 SRP model

In this study, the SRP acting on a spacecraft is calculated based on a flat plate model. This plate is perpendicular to the z^{SC} axis. Then, the SRP force acting on the spacecraft is given as follows [22]:

$$
\begin{aligned}
\boldsymbol{F}_{SRP} &= -PA(\boldsymbol{n}\cdot\boldsymbol{s}) \\
&\quad \times \left\{ \left(2(\boldsymbol{n}\cdot\boldsymbol{s})C_s + B_f C_d\right)\boldsymbol{n} + (C_d + C_a)\boldsymbol{s} \right\}
\end{aligned} \tag{10}
$$

where $\boldsymbol{n}$ is a unit vector normal to the surface of the spacecraft; $\boldsymbol{s}$ is a unit vector pointing from the spacecraft to the Sun; $B_f = 2/3$ is the Lambertian coefficient; and $P = P_0/d^2$ is the SRP acting on the surface of the spacecraft, where $P_0 \simeq 1 \times 10^{17}$ kg · m/s^2 is the solar flux constant [23]. As a result, the SRP torque can be expressed by the equation below.

$$\boldsymbol{T}_{SRP} = \boldsymbol{L}_{SRP} \times \boldsymbol{F}_{SRP} \tag{11}$$

where $\boldsymbol{L}_{SRP}$ is the position vector of the center of the SRP relative to the center of mass, which is defined as ${}^{SC}\boldsymbol{L}_{SRP} = [0, 0, L_z]^{\mathrm{T}}$. Note that the vector $\boldsymbol{n}$ is given such that $\boldsymbol{n} \cdot \boldsymbol{s} \geq 0$ is satisfied.

Eq. (10) depends on the attitude of the spacecraft, which causes the coupling of the orbital and attitude motion of the spacecraft. This coupling effect due to the SRP is usually much larger than the gravitational coupling effect described in the previous subsection.

3. Orbital motion

In this section, Sun-synchronous orbit solutions are solved by an analytical approach using Lagrange planetary equations. Although not the major contribution of this study, the derivation of the solution is described for clarity of discussion in subsequent sections.

3.1. Lagrange planetary equation

The largest gravity irregularity effect is due to the $C_{20}(= -J_2)$ term, in general, which constitutes the oblateness effect. The orbital motion of a spacecraft subject to SRP perturbation and the oblateness effect is expressed by the following averaged Lagrange planetary equations [5]:

$$\begin{aligned}
\dot{a} &= 0 \\
\dot{e} &= -K_{SRP}\sqrt{1-e^2}(\sin\omega\cos\Omega + \cos\omega\sin\Omega\cos i) \\
\dot{i} &= -K_{SRP}\frac{e}{\sqrt{1-e^2}}\cos\omega\sin\Omega\sin i \\
\dot{\Omega} &= -K_{SRP}\frac{e}{\sqrt{1-e^2}}\sin\omega\sin\Omega + \frac{K_{J_2}}{(1-e^2)^2}\cos i - N \\
\dot{\omega} &= -\frac{K_{SRP}}{e\sqrt{1-e^2}}\{(1-e^2)\cos\omega\cos\Omega - \sin\omega\sin\Omega\cos i\} \\
&\quad + \frac{K_{J_2}}{(1-e^2)^2}\left(\frac{5}{2}\sin^2 i - 2\right)
\end{aligned} \tag{12}$$

where $(a, e, i, \Omega, \omega)$ denotes the set of orbital elements defined in the Hill coordinate; N denotes the mean motion of a small body; and K_{J_2} and K_{SRP} are functions of the semi-major axis a, as follows:

$$K_{J_2} = \frac{3}{2}\cdot\frac{\sqrt{\mu}C_{20}R_a^2}{a^{\frac{7}{2}}}, \qquad K_{SRP} = \frac{3}{2}\frac{|\boldsymbol{F}_{SRP}|_{\boldsymbol{n}=\boldsymbol{s}}}{m}\sqrt{\frac{a}{\mu}} \tag{13}$$

This section assumes that the attitude of the spacecraft is always directed toward the Sun.

3.2. Sun-synchronous orbit solutions

Sun-synchronous frozen orbits can be achieved when all of the derivatives of orbital elements described in Eq. (12) are equal to zero. Several types of orbits are known to satisfy this condition. The present study investigates one of these orbits, called a near-polar terminator orbit, because this type of orbit can avoid solar eclipse and has relatively small eccentricity [5]. The orbital elements of near-polar terminator orbits can be solved as follows:

$$\begin{aligned}
a = \text{free}, \quad e = f_1(a), \quad i = f_2(a), \\
\Omega = \pm\frac{\pi}{2}, \quad \omega = \mp\frac{\pi}{2}
\end{aligned} \tag{14}$$

Here, $f_1(a)$ and $f_2(a)$ are implicit functions of the semi-major axis obtained by solving the following equations numerically:

$$\begin{aligned}
K_{SRP}\frac{e}{\sqrt{1-e^2}} + \frac{K_{J_2}}{(1-e^2)^2}\cos i = N \\
\frac{K_{SRP}}{e\sqrt{1-e^2}}\cos i - \frac{K_{J_2}}{(1-e^2)^2}\left(\frac{5}{2}\sin^2 i - 2\right) = 0
\end{aligned} \tag{15}$$

Table 3. Parameters of the Sun-synchronous orbit

Item	Symbol	Value
Semi-major axis	a	2.2 km
Eccentricity	e	0.1686
Inclination	i	94.10 deg
Longitude of the ascending node	Ω	-90 deg
Argument of periapsis	ω	90 deg
Period	τ	19.09 hr

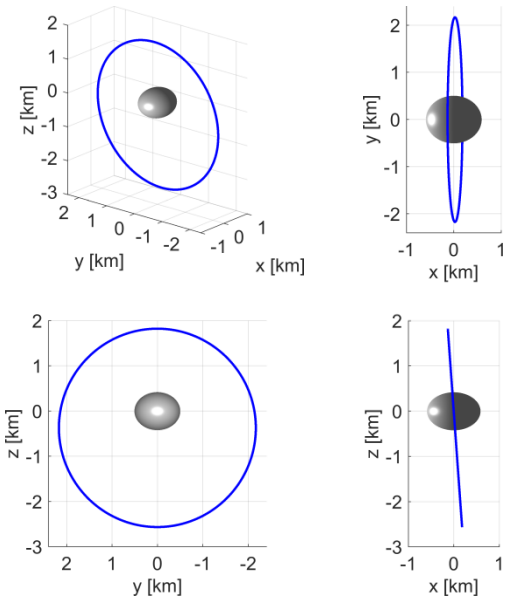

Fig. 5. Example of a Sun-synchronous orbit

An example of a Sun-synchronous orbit is provided in Fig. 5, and the parameters of the orbit are provided in Table 3. The semi-major axis is given as 2 km, and the eccentricity and inclination are solved from Eq. (15). This result demonstrates that the solution of a Sun-synchronous orbit actually exists, even when both the SRP perturbation and the oblateness effect are considered. Note that Fig. 5 simply shows an ideal elliptic orbit that is not the result of orbit propagation.

4. Attitude motion

4.1. Linearized Euler equation

Attitude motion of a spacecraft observed in an arbitrary ξ-coordinate is expressed by the Euler equations below.

$$\left.\frac{d\boldsymbol{H}}{dt}\right|_{\xi} = -\boldsymbol{\omega}_{\xi/I} \times \boldsymbol{H} + \boldsymbol{T} \tag{16}$$

Here, $d/dt|_{\xi}$ represents the time derivative in the ξ-coordinate system, and $\boldsymbol{\omega}_{\xi/\eta}$ denotes the angular velocity vector of an ξ-coordinate system relative to an η-coordinate system. In addition, the angular momentum vector $\boldsymbol{H}$ is defined as follows:

$$\boldsymbol{H} = \boldsymbol{I}\boldsymbol{\omega}_{SC/I} + \boldsymbol{h} \tag{17}$$

where $\boldsymbol{h}$ is an internal angular momentum vector of the spacecraft provided by internal actuators, such as reaction wheels. It is assumed that $\boldsymbol{h}$ has only the z component in terms of the spacecraft-fixed coordinate, which yields the equation below.

$${}^{SC}\boldsymbol{h} = {}^{SF}\boldsymbol{h} = [0, 0, h_z]^{\mathrm{T}} \tag{18}$$

Throughout this paper, h_z is specified as a constant variable, which means that the spacecraft has constant bias angular momentum with no feedback control. The moment of inertia tensor $\boldsymbol{I}$ is a constant variable when it is expressed in the spacecraft-fixed coordinate. It is also constant when it is expressed in the spin-free coordinate, if the spacecraft's shape is axisymmetrical. Accordingly, the moment of inertia tensor can be expressed as follows:

$${}^{SC}\boldsymbol{I} = \begin{bmatrix} I_x & 0 & 0 \\ 0 & I_y & 0 \\ 0 & 0 & I_z \end{bmatrix}, \quad {}^{SF}\boldsymbol{I} = \begin{bmatrix} I_r & 0 & 0 \\ 0 & I_r & 0 \\ 0 & 0 & I_z \end{bmatrix} \tag{19}$$

where $I_r \equiv I_x = I_y$. As a result, when it is expressed in the spacecraft-fixed or spin-free coordinate, Eq. (16) can be rewritten as the following equation:

$$\boldsymbol{I}\left.\frac{d\boldsymbol{\omega}_{SC/I}}{dt}\right|_{\xi} = -\boldsymbol{\omega}_{\xi/I} \times \left(\boldsymbol{I}\boldsymbol{\omega}_{SC/I} + \boldsymbol{h}\right) + \boldsymbol{T} \tag{20}$$

To achieve Sun-tracking attitude motion, it is essential to understand the dynamics regarding the in-plane Sun angle θ and the out-of-plane Sun angle ϕ. Thus, the attitude motion observed in the spin-free coordinate is analyzed in this section. The equation of attitude motion expressed in the spin-free coordinate is given by the equation below (ref. Appendix A).

$$\begin{bmatrix} I_r\ddot{\phi} \\ I_r\ddot{\theta} \\ I_z\dot{\Omega}_z \end{bmatrix} = \begin{bmatrix} -(I_z\Omega_z + h_z)\left(\dot{\theta} - N\right) \\ (I_z\Omega_z + h_z)\dot{\phi} \\ 0 \end{bmatrix} + {}^{SF}\boldsymbol{T}_{GG} + {}^{SF}\boldsymbol{T}_{SRP} \tag{21}$$

where ${}^{SF}\boldsymbol{\omega}_{SC/SF} = [0, 0, \Omega_z]^{\mathrm{T}}$.

When GG torque due to the higher-order gravity term is assumed negligible, $\boldsymbol{T}_{GG}$ can be expressed as follows, based on Eqs. (9) and (61):

$$\boldsymbol{T}_{GG} = -\frac{3\mu}{|\boldsymbol{r}|^5}\boldsymbol{r} \times \boldsymbol{I}\boldsymbol{r} \tag{22}$$

Position vector ${}^{SF}\boldsymbol{r}$ can be expressed with the orbital elements as follows:

$${}^{H}\boldsymbol{r} = \boldsymbol{R}_z(-\Omega)\boldsymbol{R}_x(-i)\boldsymbol{R}_z(-\omega - f)\begin{bmatrix} r \\ 0 \\ 0 \end{bmatrix} \tag{23}$$

$${}^{SF}\boldsymbol{r} = {}^{SF}\boldsymbol{C}_{SP}{}^{SP}\boldsymbol{C}_{H}{}^{H}\boldsymbol{r} \tag{24}$$

where r is also a function of orbital elements, which satisfies the equation below.

$$r = \frac{a(1 - e^2)}{1 + e\cos f} \tag{25}$$

Because ${}^{SF}\boldsymbol{r}$ is a function of the true anomaly f, ${}^{SF}\boldsymbol{T}_{GG}$ is a time-dependent variable. However, the GG torque can be averaged over one period of the orbit around a small body as given by the equation below.

$$\begin{aligned} {}^{SF}\overline{\boldsymbol{T}}_{GG} &= \frac{1}{\tau}\int_0^{\tau} {}^{SF}\boldsymbol{T}_{GG}\,dt \\ &= \frac{(1 - e^2)^{\frac{3}{2}}}{2\pi}\int_0^{2\pi} \frac{{}^{SF}\boldsymbol{T}_{GG}(f)}{(1 + e\cos f)^2}\,df \end{aligned} \tag{26}$$

where τ denotes the orbital period. When the orbital element parameters in Eq. (26) satisfy Eq. (14), which is the Sun-synchronous frozen orbit condition, those orbital parameters are constant, and ${}^{SF}\overline{\boldsymbol{T}}_{GG}$ is a time-independent function. From Eqs. (22)–(26), this averaged GG torque has the following explicit form:

$$ {}^{SF}\bar{\boldsymbol{T}}_{GG} = \frac{3\mu(I_z - I_r)}{4a^3(1-e^2)^{\frac{3}{2}}} \begin{bmatrix} c_1\phi + c_2\theta + c_4 \\ c_2\phi + c_3\theta + c_5 \\ 0 \end{bmatrix} \quad (27) $$

where

$$ \begin{aligned} c_1 &= 2(-\sin^2 i \sin^2 \Omega + \cos^2 i) \\ c_2 &= -\sin 2i \cos \Omega \\ c_3 &= 2\sin^2 i \cos 2\Omega \\ c_4 &= -\sin 2i \sin \Omega \\ c_5 &= \sin^2 i \sin 2\Omega \end{aligned} \quad (28) $$

It is important to reiterate that ϕ and θ are assumed to be small, such that Eq. (27) is linearized with respect to ϕ and θ. Using this small angle approximation, the SRP torque can be expressed in the spin-free coordinate by the equation below, based on Eqs. (10)–(11).

$$ {}^{SF}\boldsymbol{T}_{SRP} = PAL(1 - C_s) \begin{bmatrix} \phi \\ \theta \\ 0 \end{bmatrix} \quad (29) $$

Considering z components of Eqs. (21), (27), and (29), Ω_z is a constant parameter. Given that the spacecraft is a three-axis stabilized non-spinning spacecraft, $\Omega_z = 0$ always holds. Then, the following two-dimensional differential equation is derived:

$$ I_r \begin{bmatrix} \ddot{\phi} \\ \ddot{\theta} \end{bmatrix} = h_z \begin{bmatrix} -\dot{\theta} + N \\ \dot{\phi} \end{bmatrix} + \begin{bmatrix} {}^{SF}\bar{T}_{GG,x} \\ {}^{SF}\bar{T}_{GG,y} \end{bmatrix} + \begin{bmatrix} {}^{SF}T_{SRP,x} \\ {}^{SF}T_{SRP,y} \end{bmatrix} \quad (30) $$

Based on this averaged linearized Euler equation, dynamical characteristics of Sun-tracking attitude motion can be well understood by several analytical analyses, as shown in later subsections.

4.2. Torque field

The attitude motion of a spacecraft is composed of low frequency motion called precession and high frequency motion called nutation. In general, the time dependence of precession is much smaller than nutation. Therefore, when the nutation motion is ignored so that only the precession motion is considered, the rates of change in ϕ and θ can be approximated as constant, yielding $\ddot{\phi} \simeq \ddot{\theta} \simeq 0$ [18]. This assumption can also be made for the situation where the spacecraft is always in pure rotation [9]. Then, Eq. (30) simplifies to the following first-order differential equation:

$$ h_z \begin{bmatrix} \dot{\theta} \\ \dot{\phi} \end{bmatrix} = \begin{bmatrix} h_z N \\ 0 \end{bmatrix} + \begin{bmatrix} {}^{SF}\bar{T}_{GG,x} \\ -{}^{SF}\bar{T}_{GG,y} \end{bmatrix} + \begin{bmatrix} {}^{SF}T_{SRP,x} \\ -{}^{SF}T_{SRP,y} \end{bmatrix} \quad (31) $$

The first term of the right-hand side represents the inertial torque due to the rotational motion of the coordinate itself. The second and third terms correspond to the GG torque and the SRP torque, which are functions of ϕ and θ given by Eqs. (27) and (29), respectively. Therefore, Eq. (31) expresses the velocity field in the ϕ-θ plane as the summation of the inertial torque, GG torque, and SRP torque.

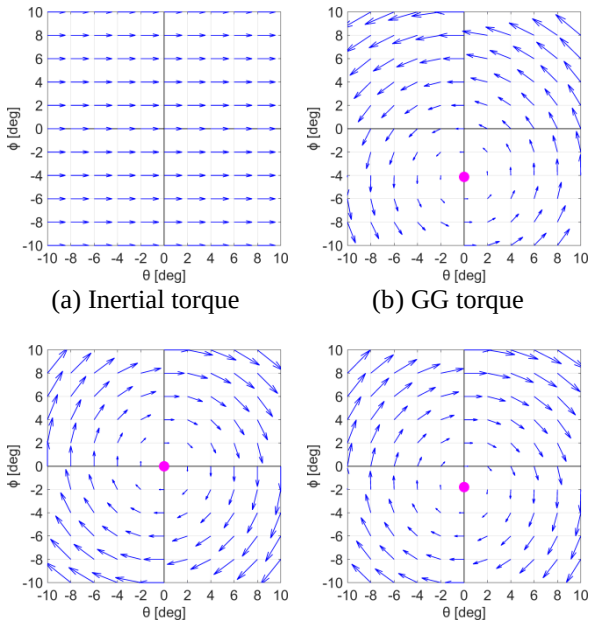

(a) Inertial torque (b) GG torque

(c) SRP torque (d) Resultant torque

Fig. 6. Torque fields

Fig. 6 shows the torque fields of these torques and the resultant torque field expressed in the ϕ-θ plane, in which the origin corresponds to the direction of the Sun. Inertia torque simply depends on the bias angular momentum h_z (not on ϕ nor θ), as shown in Fig. 6a. Fig. 6b shows the averaged GG torque applied on a spacecraft moving in the Sun-synchronous orbit provided in Fig. 5. The SRP torque has a concentric torque field, the center of which is located at the origin, as shown in Fig. 6c. As a result, the resultant torque field, which is illustrated in Fig. 6d, can be obtained as the superposition of the three torque fields. In this figure, the bias momentum is given as $h_z = 2\,\mathrm{Nms}$. Here, magenta points in these figures represent equilibrium points, where the torque is identical to zero.

As previously mentioned, Eq. (31) describes the precession motion of a spacecraft. Therefore, Fig. 6d implies that the spacecraft can always be pointed in the Sun direction by precessing around the equilibrium direction located close to the Sun, which means Sun-tracking attitude motion can be achieved in this system.

4.3. Stability conditions of Sun-tracking attitude motion

The second-order differential equations in Eq. (30) can be rewritten as the following first-order differential equations:

$$\frac{d}{dt}\begin{bmatrix}\phi\\ \theta\\ \dot{\phi}\\ \dot{\theta}\end{bmatrix}=\begin{bmatrix}0 & 0 & 1 & 0\\ 0 & 0 & 0 & 1\\ C_1 & C_2 & 0 & -h_z/I_r\\ C_2 & C_3 & h_z/I_r & 0\end{bmatrix}\begin{bmatrix}\phi\\ \theta\\ \dot{\phi}\\ \dot{\theta}\end{bmatrix}+\begin{bmatrix}0\\ 0\\ C_4+h_zN/I_r\\ C_5\end{bmatrix} \tag{32}$$

where

$$p=\frac{PAL(1-C_s)}{I_r},\quad q=\frac{3\mu(I_z-I_r)}{4a^3(1-e^2)^{\frac{3}{2}}I_r},$$
$$C_1=p+qc_1,\quad C_2=qc_2,$$
$$C_3=p+qc_3,\quad C_4=qc_4,\quad C_5=qc_5 \tag{33}$$

Substitution of $\ddot{\phi}=\ddot{\theta}=\dot{\phi}=\dot{\theta}=0$ into Eq. (32) yields the following equilibrium solution:

$$\phi_{eq}=\frac{C_2C_5-C_3(C_4+h_zN/I_r)}{C_1C_3-C_2^2}$$
$$\theta_{eq}=\frac{-C_1C_5+C_2(C_4+h_zN/I_r)}{C_1C_3-C_2^2} \tag{34}$$

This equilibrium point (ϕ_{eq},θ_{eq}) is shown as the magenta point in Fig. 6d. As shown in Eq. (34), the position of an equilibrium point depends on the physical parameters of the spacecraft and the small body, the orbital elements, and the magnitude of bias angular momentum.

The stability of the motion around an equilibrium point, which can also be regarded as the stability of the Sun-tracking attitude motion, is analyzed based on the following characteristic equation:

$$\lambda^4+\alpha\lambda^2+\beta=0 \tag{35}$$

Here, λ represents the eigenvalues of the 4×4 matrix in Eq. (32), and α and β are defined as follows:

$$\alpha=\left(\frac{h_z}{I_r}\right)^2-(C_1+C_3)$$
$$\beta=C_1C_3-C_2^2 \tag{36}$$

Given the form of Eq. (35), the Sun-tracking motion exhibits stability only when the eigenvalues have two conjugate pairs of pure-imaginary values, as expressed by the following condition:

$$\alpha^2-4\beta>0\ \text{ and }\ \alpha>0\ \text{ and }\ \beta>0 \tag{37}$$

The necessary and sufficient conditions of Eq. (37) can be expressed by the two inequalities below.

$$C_1C_3-C_2^2>0 \tag{38}$$

$$h_z>I_r\sqrt{C_1+C_3+2\sqrt{C_1C_3-C_2^2}} \tag{39}$$

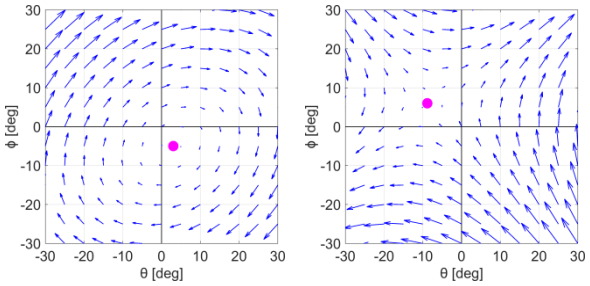

(a) Stable case (b) Unstable case

Fig. 7. Stability of an equilibrium point

Eq. (38) is a condition regarding the formulations of the GG torque and the SRP torque. This inequality indicates that an equilibrium point must be stable to ensure the stability of the Sun-tracking attitude motion. In other words, the flow of a torque field must not be divergent. Fig. 7 shows examples of a stable equilibrium point, which satisfies $C_1C_3-C_2^2>0$, and an unstable equilibrium point, which satisfies $C_1C_3-C_2^2<0$. As illustrated in these figures, the stable case corresponds to a center point and the unstable case corresponds to a saddle point. Note that Fig. 7 depicts an example of torque field assuming an arbitrary orbit, but not a Sun-synchronous orbit. Eq. (39) is a constraint on bias angular momentum, which expresses that the magnitude of momentum must be sufficiently large to achieve stable Sun-tracking attitude motion. Given the system and the Sun-synchronous orbit specified using the parameters provided in Table 1 – Table 3, the solution to Eq. (39) is $h_z>0.115$ Nms. It appears that this constraint is realistic, given the example of the Hayabusa 2 spacecraft, which is operated with a nominal angular momentum of $h_z=3.09$ Nms [18].

When an equilibrium point is stable and a spacecraft possesses sufficient bias angular momentum, the Sun-tracking motion is stable, and the eigenvalues can be expressed as follows:

$$\lambda=\pm i\omega_p,\pm i\omega_n \tag{40}$$

Here, ω_p is the frequency of precession motion, and ω_n is the frequency of nutation motion, which are calculated as follows:

$$\omega_p=\sqrt{\frac{\alpha-\sqrt{\alpha^2-4\beta}}{2}},\quad \omega_n=\sqrt{\frac{\alpha+\sqrt{\alpha^2-4\beta}}{2}} \tag{41}$$

5. Coupled orbit-attitude motion

5.1. Hill's equation and Euler equation

Orbital motion is analyzed by introducing the Lagrange planetary equation in Section 2, and attitude motion is analyzed by introducing the linearized Euler

equation in Section 3. Although these models allow analytical analyses to understand the dynamics behind the orbit-attitude coupled system, they are formulated with approximations that involve linearization and averaging. Therefore, in this section, a non-linear orbit-attitude coupled equation of motion is derived for more precise analyses to verify the validity of the analytical solutions obtained in the previous sections.

The orbital motion of a spacecraft in the proximity of a small body moving in a circular orbit around the Sun can be modelled using Hill's equation below [23, 26].

$$\begin{aligned} m\ddot{\boldsymbol{r}} + 2m\boldsymbol{\omega}_{H/I} \times \dot{\boldsymbol{r}} + m\boldsymbol{\omega}_{H/I} \times \left(\boldsymbol{\omega}_{H/I} \times \boldsymbol{r}\right) \\ = m|\boldsymbol{\omega}_{H/I}|^2(3(\boldsymbol{d}\cdot\boldsymbol{r})\boldsymbol{d} - \boldsymbol{r}) + \boldsymbol{F}_G + \boldsymbol{F}_{SRP} \end{aligned} \quad (42)$$

where $\boldsymbol{d}$ is a unit vector pointing from the Sun to the small body. This equation is expressed in the Hill coordinate as follows:

$$m\begin{bmatrix}\ddot{x}\\ \ddot{y}\\ \ddot{z}\end{bmatrix} = m\begin{bmatrix}2N\dot{y} + 3N^2x\\ -2N\dot{x}\\ -N^2z\end{bmatrix} + {}^{H}\boldsymbol{F}_G + {}^{H}\boldsymbol{F}_{SRP} \quad (43)$$

The gravitational force ${}^{H}\boldsymbol{F}_G$ and the SRP force ${}^{H}\boldsymbol{F}_{SRP}$ are calculated from Eqs. (8), (10), and (60), which incorporate the effect of the spacecraft's attitude.

On the other hand, the attitude motion of the spacecraft is modelled by Eq. (20), and the motion observed in the spacecraft-fixed coordinate can be expressed by the equation below.

$$\begin{bmatrix}I_x\dot{\omega}_x\\ I_y\dot{\omega}_y\\ I_z\dot{\omega}_z\end{bmatrix} = \begin{bmatrix}(I_y - I_z)\omega_y\omega_z - h_z\omega_y\\ (I_z - I_x)\omega_x\omega_z + h_z\omega_x\\ (I_x - I_y)\omega_x\omega_y\end{bmatrix} + {}^{SC}\boldsymbol{T}_{GG} + {}^{SC}\boldsymbol{T}_{SRP} \quad (44)$$

where ${}^{SC}\boldsymbol{\omega}_{SC/I} = [\omega_x, \omega_y, \omega_z]^{\mathrm{T}}$. The GG torque ${}^{SC}\boldsymbol{T}_{GG}$ and the SRP torque ${}^{SC}\boldsymbol{T}_{SRP}$ are calculated from Eqs. (9), (11), and (61). Because the GG torque depends on the position of the spacecraft relative to the small body, Eqs. (43) and (44) form coupled orbit-attitude equations of motion.

Considering a 2-1-3 rotation sequence from the Sun-pointing coordinate to the spacecraft-fixed coordinate with an Euler angle set of (ϕ, θ, ψ), the relationship between angular velocities and Euler angles can be expressed as follows (ref. Appendix B):

$$\begin{bmatrix}\dot{\phi}\\ \dot{\theta}\\ \dot{\psi}\end{bmatrix} = \begin{bmatrix}\omega_x\cos\psi - \omega_y\sin\psi\\ \left(\omega_x\sin\psi + \omega_y\cos\psi\right)\sec\phi + N\\ \left(\omega_x\sin\psi + \omega_y\cos\psi\right)\tan\phi + \omega_z\end{bmatrix} \quad (45)$$

Then, Eqs. (43)–(45) and the relationship between position and velocity provide a total of twelve equations, such that the following twelve variables can be obtained using numerical propagation:

$$\left(x, y, z, \dot{x}, \dot{y}, \dot{z}, \phi, \theta, \psi, \omega_x, \omega_y, \omega_z\right) \quad (46)$$

5.2. Propagation of orbit-attitude coupled motion

The simulated results obtained for orbit-attitude coupled motion are provided in Fig. 8 – Fig. 10. These results show the coupled motions of a spacecraft orbiting in the Sun-synchronous orbit shown in Fig. 5, which satisfies the stability condition given by Eq. (38). The simulations are performed for different bias angular momentum values, which are $h_z = 2$, 0.25, and 0.04 Nms. The former two cases satisfy the stability condition given by Eq. (39), while the last case does not satisfy this condition. These motions are propagated for 100 days.

Fig. 8 demonstrates that a Sun-synchronous orbit with Sun-tracking attitude motion can actually be achieved if a spacecraft has sufficient bias angular momentum. Fig. 8a illustrates the orbital motion in the Hill coordinate. It can be observed from this figure that the orbital shape and geometry remain constant, and thus, this orbit is Sun-synchronous. Fig. 8b contains a visual representation of the attitude trajectory in the ϕ-θ plane, in which the origin corresponds to the Sun direction. This figure indicates that the spacecraft is always directed toward the Sun, with a slight oscillation of several degrees around the equilibrium point. The blue arrows in Fig. 8b represent the torque field calculated from Eq. (31). This result demonstrates that the precession motion of the spacecraft varies along the flow of the torque field. As observed from the enlarged view in the red box, the nutation motion also appears as a trajectory with many loops, and it is winded mainly because of the variation in GG torque. Fig. 8c gives the history of the spin phase ψ, and, as depicted, the phase varies less than 5 deg over 100 days.

These observations indicate that the proposed method to implement both a Sun-synchronous orbit and Sun-tracking motion is feasible even when the dynamical system around a small body is strongly perturbed and coupled. Moreover, the result demonstrates that the analytical solutions obtained in Section 2 and 3 are valid approximations describing the dynamics of the complex system. It is also important to reiterate that the bias angular momentum is kept constant in this simulation, and no feedback control is applied. Thus, implementation of the proposed method is expected to be simple.

Fig. 9 shows a case in which bias angular momentum is smaller than the previous case. Although the stability condition given by Eq. (38) is still satisfied, the attitude motion is less stable, as shown in Fig. 9b. Incidentally, the positions of equilibrium points differ

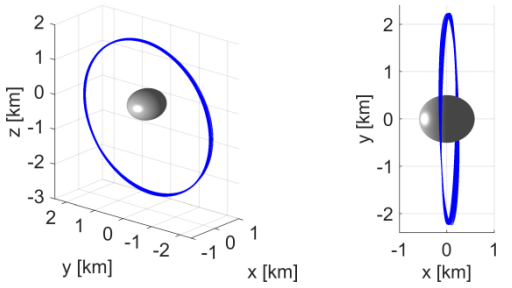

(a) Orbital motion

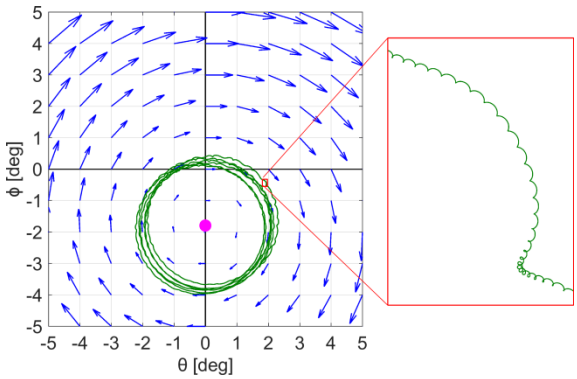

(b) Attitude motion: Sun angle

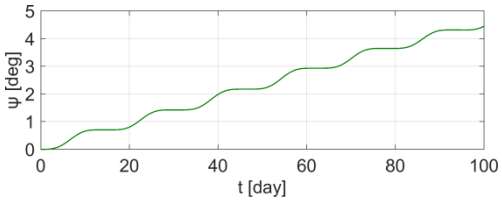

(c) Attitude motion: spin phase

Fig. 8. Orbit-attitude coupled motion, $h_z = 2$ Nms

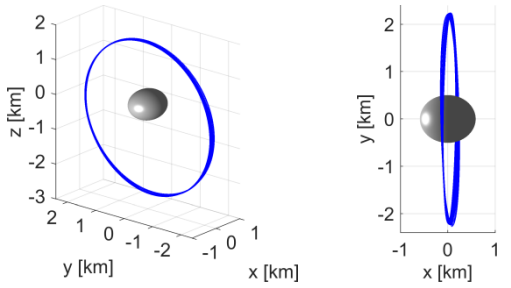

(a) Orbital motion

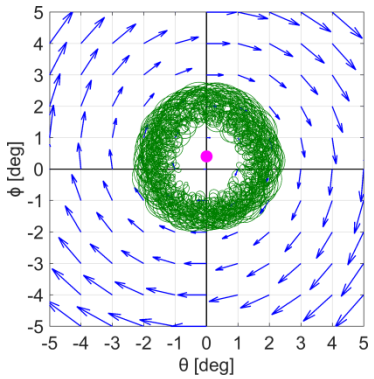

(b) Attitude motion: Sun angle

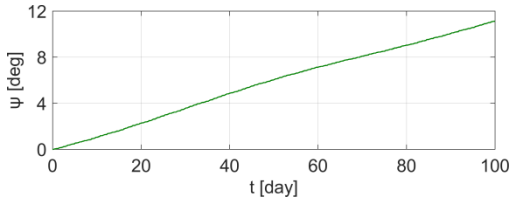

(c) Attitude motion: spin phase

Fig. 9. Orbit-attitude coupled motion, $h_z = 0.25$ Nms

between Fig. 8b and Fig. 9b, because these positions depend on the magnitude of bias angular momentum.

When the magnitude of angular momentum further decreases and the stability condition given by Eq. (38) is violated, orbit-attitude coupled motion becomes unstable. Fig. 10b illustrates that Sun angles ϕ and θ are no longer close to zero. This unstable attitude motion causes large variations in the SRP force applied to the spacecraft, resulting in the divergence of orbital motion, as shown in Fig. 10a. This observation implies that, in order to achieve a Sun-synchronous orbit with Sun-tracking attitude motion, it is essential to fulfill certain initial conditions regarding both the orbital and the attitude motion.

5.3. Frequency analysis of orbit-attitude coupled motion

A Sun-synchronous frozen orbit is not a periodic orbit, in the strict sense, but is rather quasi-periodic. This is because the orbit is subject to periodic perturbations, which are not considered in the averaged Lagrange planetary equation [2]. Moreover, when coupling effects are considered, the periodicity of orbital motion is affected by the frequency of attitude motion, and vice versa. Consequently, both the orbital and the attitude motion consist of multiple frequency components, making it difficult to characterize those motions using only the time-domain history.

Therefore, to identify the characteristics of orbit-attitude coupled motion, frequency analysis is performed using discrete Fourier transform (DFT). In previous research, DFT has been used to deduce fundamental characteristics (for example, the stability) of quasi-periodic orbits [26, 27]. This analysis method is an effective numerical approach with low computational cost. By applying the same approach to the present study, the frequency components of coupled motion can be extracted from the propagated discrete data.

Let u denote an arbitrary state variable regarding the orbit-attitude coupled motion. Then, this variable can be

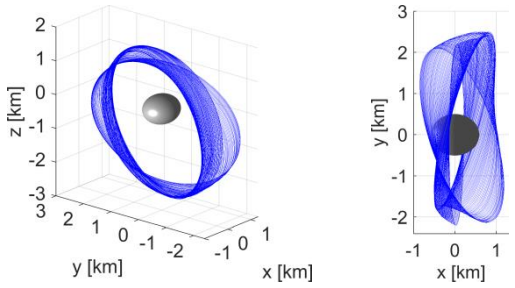

(a) Orbital motion

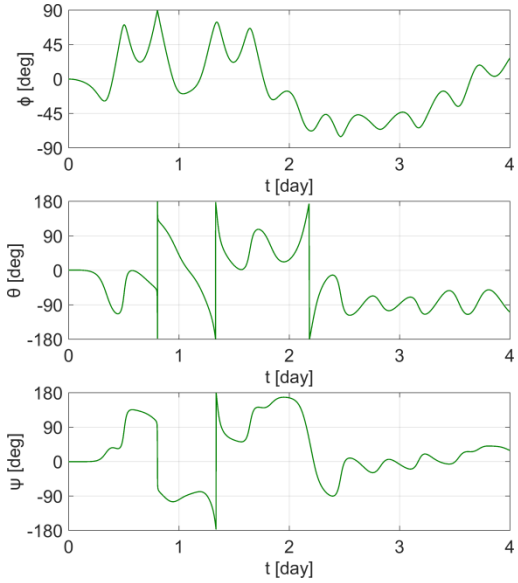

(b) Attitude motion ($0 \leq t \leq 4$ days)

Fig. 10. Orbit-attitude coupled motion, $h_z = 0.04$ Nms

decomposed into multiple frequency components as follows:

$$u_j = \sum_{k=0}^{N_{DFT}-1} A_k e^{i\omega_k t_j} \quad (j = 0, 1, \ldots, N_{DFT} - 1) \quad (47)$$

where

$$\omega_k = \frac{2\pi}{T_{DFT}} k, \qquad t_j = \frac{T_{DFT}}{N_{DFT}} j \quad (48)$$

Here, N_{DFT} denotes the number of sample points, and T_{DFT} denotes the total time span. Then, the amplitude A_k of the corresponding frequency ω_k is obtained by the following DFT calculation:

$$A_k = \frac{1}{N_{DFT}} \sum_{j=0}^{N_{DFT}-1} u_j e^{-i\omega_k t_j} \quad (k = 0, 1, \ldots, N_{DFT} - 1) \quad (49)$$

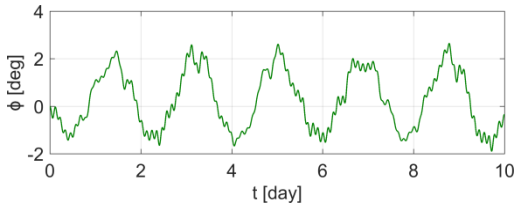

(a) Time domain history ($0 \leq t \leq 10$ days)

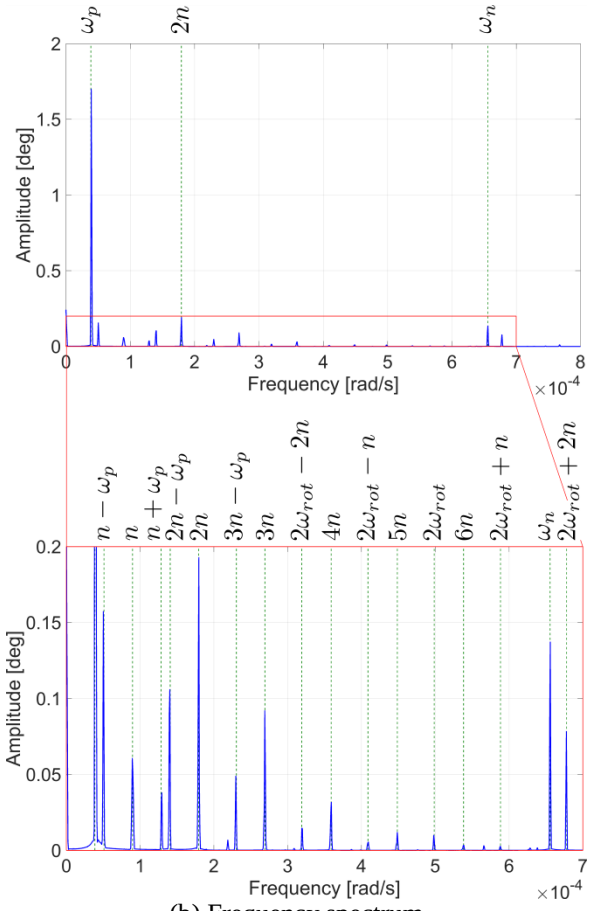

(b) Frequency spectrum

Fig. 11. Frequency analysis of orbit-attitude coupled motion

An example result of DFT analysis is shown in Fig. 11. Fig. 11a provides the time history of the in-plane Sun angle ϕ when $h_z = 0.25$ Nms, which corresponds to the simulation shown in Fig. 9. It can be observed from this figure that the attitude angle varies with multiple frequencies. When DFT is applied to this time-domain history, Fig. 11b is obtained as the frequency spectrum. This figure illustrates frequencies ω_k of the attitude motion, and their magnitudes $|A_k|$. In this computation, $N_{DFT} = 2^{20}$ and $T_{DFT} = 100$ day. Among the multiple peaks appearing in Fig. 11b, the three major peaks correspond to the following: the frequency of precession motion ω_p, which is given by Eq. (41); the

frequency of nutation motion ω_n, which is given by Eq. (41); double the mean motion n, which is calculated numerically by detecting the spacecraft crossing the x-z plane. Other peaks in the figure are expressed as combinations of ω_p, ω_n, n, and ω_{rot}. Here, $\omega_{rot} = 2\pi/T_{rot}$ is the rotational spin rate of the small-body. This result implies that the propagated motion contains both orbit-related and attitude-related frequency components, due to the coupling effect. The result also indicates that, although the strongly perturbed orbit-attitude coupled dynamics exhibit complex behavior, the motion can be characterized by analytical theory.

5.4. Dynamic environment around a small body

The simulation results presented in the previous subsections imply that the orbit-attitude coupling effect influences the motion of a spacecraft around a small body. This subsection provides a more detailed analysis and reveals which forces or torques acting on a spacecraft are dominant.

Fig. 12 provides the magnitudes of forces and torques applied to the spacecraft during a single orbital period. This figure corresponds to the simulation illustrated in Fig. 8, which is a stable case. Here, C_{mn} represents the gravitational force/torque due to the corresponding spherical harmonics coefficient. Fig. 12a shows that the zeroth-order gravitational force is the largest. The SRP force and the second-order gravitational forces, both of which substantially perturb the orbital motion, have almost the same order of magnitude. As observed from the figure, the fourth-order gravitational forces, the solar tidal force, and the gravitational coupling effect are much smaller. On the other hand, Fig. 12b shows that the SRP torque and the GG torque due to the zeroth-order gravitational term are dominant. The second-order GG torque has a magnitude that is approximately 1-10% of those of the major torques, while the GG torque due to the solar gravity is negligible.

Fig. 13 shows forces and torques histories of the simulation illustrated in Fig. 10, which is an unstable case. Comparing Fig. 12a and Fig. 13a, it is apparent that the variation in SRP force is much larger in the unstable case. This variation is caused by unstable attitude motion, as shown in Fig. 10b, and causes unstable orbital motion, as shown in Fig. 10a.

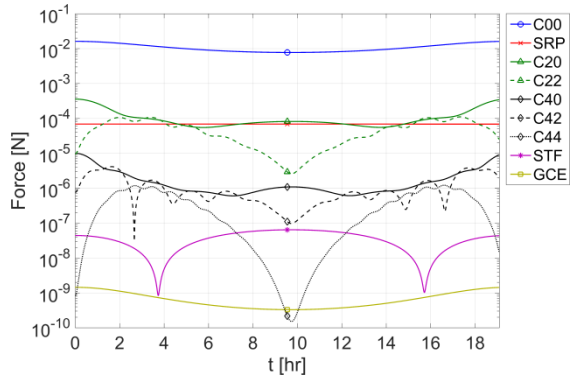

(a) Force history (STF: solar tidal force, GCE: gravitational coupling effect)

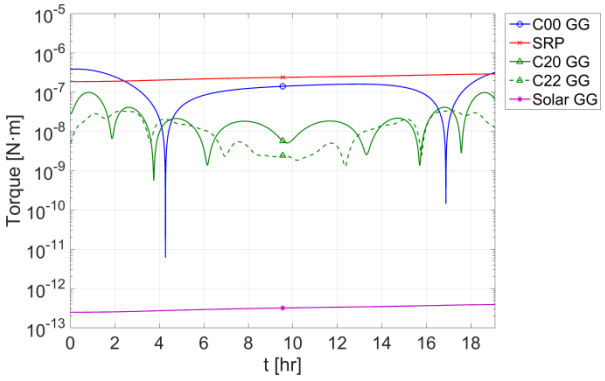

(b) Torque history

Fig. 12. The forces and torques acting on the spacecraft during one orbital period, $h_z = 2$ Nms

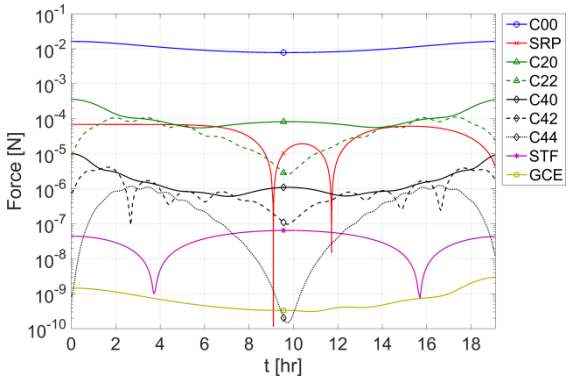

(a) Force history (STF: Solar tidal force, GCE: gravitational coupling effect)

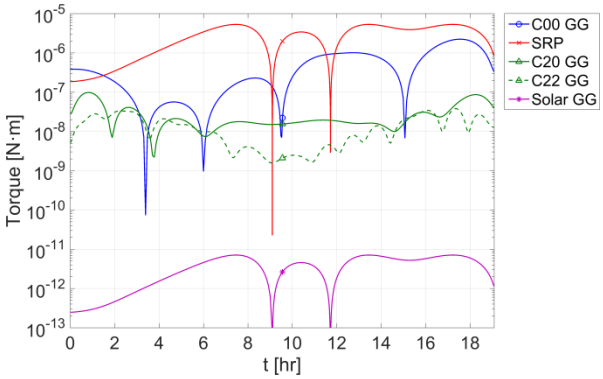

(b) Torque history

Fig. 13. The forces and torques acting on the spacecraft during one orbital period, $h_z = 0.04$ Nms

These results show that the motion of a spacecraft around a small body is perturbed by both SRP and gravitational effects. Moreover, via these perturbations, the orbital and attitude motion are coupled and significantly influence each other. The important point is that even in such a complex system, stationary orbit-attitude coupled motion can be achieved without active control if the initial conditions of orbital and attitude motion are designed properly.

6. Conclusions

The motion of a spacecraft in the proximity of a small body is significantly perturbed by the solar radiation pressure (SRP) and the gravity irregularity. In such a strongly perturbed environment, the coupling effect of the orbital and attitude motion exerts a large influence and can cause divergence of these motions. To solve this problem, the present study investigated the implementation of Sun-synchronous orbits with Sun-tracking attitude motion.

First, the orbital and attitude motion were analyzed separately, and the conditions to achieve Sun-synchronous orbits and Sun-tracking attitude motion were investigated. Although the coupled system is complex, analytical solutions of the proposed motion were successfully obtained by applying averaging and linearization. Next, the orbit-attitude coupled motion was propagated based on more precise non-linear equations of motion. This step demonstrated that if the initial conditions of orbital and attitude motions are given properly, both a Sun-synchronous orbit and Sun-tracking attitude motion can be achieved without requiring any active control.

These novel orbit-attitude coupled dynamics can reduce the use of orbit and attitude control system, thereby reducing the weight of a spacecraft and prolonging the life time of the mission. It is therefore concluded that the proposed natural orbit-attitude coupled dynamics is feasible and useful for real small-body missions.

Acknowledgements

This work was supported by JSPS KAKENHI Grant Number 15J06932 and 26289325.

Appendix A: Derivation of Eq. (21)

Considering a 2-1-3 rotation sequence from the Sun-pointing coordinate to the spin-free coordinate with an Euler angle set of $(\phi, \theta, 0)$, the angular momentum vector can be expressed as follows, according to the kinematic equations [9]:

$$ {}^{SF}\boldsymbol{\omega}_{SF/SP} = \begin{bmatrix} \dot{\phi} \\ \dot{\theta}\cos\phi \\ -\dot{\theta}\sin\phi \end{bmatrix} \simeq \begin{bmatrix} \dot{\phi} \\ \dot{\theta} \\ 0 \end{bmatrix} \tag{50} $$

Here, it is assumed that $\phi, \theta \ll 1$, which means that the z axis of the spacecraft-fixed coordinate points very closely in the Sun direction. Under this assumption, the following equation holds from Eq. (4):

$$ {}^{SF}\boldsymbol{\omega}_{SP/I} = {}^{SF}\boldsymbol{C}_{SP}\,{}^{SP}\boldsymbol{\omega}_{SP/I} \simeq \begin{bmatrix} 0 \\ -N \\ 0 \end{bmatrix} \tag{51} $$

where N denotes the mean motion of the revolution orbit of the small body around the Sun, and thus, ${}^{SP}\boldsymbol{\omega}_{SP/I} \simeq [0, -N, 0]^{\mathrm{T}}$. From Eqs. (50) and (51), the following equation can be obtained:

$$ {}^{SF}\boldsymbol{\omega}_{SF/I} = {}^{SF}\boldsymbol{\omega}_{SF/SP} + {}^{SF}\boldsymbol{\omega}_{SP/I} \simeq \begin{bmatrix} \dot{\phi} \\ \dot{\theta} - N \\ 0 \end{bmatrix} \tag{52} $$

Letting Ω_z denote the angular velocity of the spacecraft-fixed coordinate relative to the spin-free coordinate yields ${}^{SF}\boldsymbol{\omega}_{SC/SF} = [0, 0, \Omega_z]^{\mathrm{T}}$. Then, the following equation is obtained from Eq. (52):

$$ {}^{SF}\boldsymbol{\omega}_{SC/I} = {}^{SF}\boldsymbol{\omega}_{SC/SF} + {}^{SF}\boldsymbol{\omega}_{SF/I} \simeq \begin{bmatrix} \dot{\phi} \\ \dot{\theta} - N \\ \Omega_z \end{bmatrix} \tag{53} $$

From Eqs. (20), (52), and (53), the attitude motion observed in the spin-free coordinate can be expressed in the same coordinate by Eq. (21).

Appendix B: Derivation of Eq. (45)

Considering a 2-1-3 rotation sequence from the Sun-pointing coordinate to the spacecraft-fixed coordinate with an Euler angle set of (ϕ, θ, ψ), the relationship between angular velocities and Euler angles can be expressed as the equation below [9].

$$ \begin{aligned} \dot{\phi} &= \tilde{\omega}_x \cos\psi - \tilde{\omega}_y \sin\psi \\ \dot{\theta} &= \left(\tilde{\omega}_x \sin\psi + \tilde{\omega}_y \cos\psi\right)\sec\phi \\ \dot{\psi} &= \left(\tilde{\omega}_x \sin\psi + \tilde{\omega}_y \cos\psi\right)\tan\phi + \tilde{\omega}_z \end{aligned} \tag{54} $$

where ${}^{SC}\boldsymbol{\omega}_{SC/SP} = \left[\tilde{\omega}_x, \tilde{\omega}_y, \tilde{\omega}_z\right]^{\mathrm{T}}$. Considering angular velocity vectors among the inertial, Sun-pointing, and spacecraft-fixed coordinate, the following equation holds:

$$ \begin{aligned} {}^{SC}\boldsymbol{\omega}_{SC/SP} &= {}^{SC}\boldsymbol{\omega}_{SC/I} - {}^{SC}\boldsymbol{C}_{SP}\,{}^{SP}\boldsymbol{\omega}_{SP/I} \\ &\Leftrightarrow \begin{cases} \tilde{\omega}_x = \omega_x + N\cos\phi\sin\psi \\ \tilde{\omega}_y = \omega_y + N\cos\phi\cos\psi \\ \tilde{\omega}_z = \omega_z + N\sin\phi \end{cases} \end{aligned} \tag{55} $$

Then, substitution of Eq. (55) into Eq. (54) yields Eq. (45).

Appendix C: Explicit forms of forces and torques

The spherical harmonics coefficients are defined as follows [23]:

$$C_{20}=\frac{1}{10R_a^2}\{2R_c^2-(R_a^2+R_b^2)\},\quad C_{22}=\frac{1}{20R_a^2}(R_a^2-R_b^2)$$
$$C_{40}=\frac{15}{7}(C_{20}^2+2C_{22}^2),\quad C_{42}=\frac{5}{7}C_{20}C_{22},\quad C_{44}=\frac{5}{28}C_{22}^2 \tag{56}$$

Considering the vector form of the Taylor series, the following equation can be derived:

$$\begin{aligned} f(\boldsymbol{R}) &= f(\boldsymbol{r}+\boldsymbol{\rho}) \\ &\simeq f(\boldsymbol{r})+\nabla f(\boldsymbol{r})\cdot\boldsymbol{\rho}+\frac{1}{2}\boldsymbol{\rho}^{\mathrm{T}}\nabla^2 f(\boldsymbol{r})\boldsymbol{\rho} \end{aligned} \tag{57}$$

where

$$\nabla f(\boldsymbol{r})=\left.\frac{\partial f}{\partial \boldsymbol{R}}\right|_{\boldsymbol{R}=\boldsymbol{r}},\quad \nabla^2 f(\boldsymbol{r})=\left.\frac{\partial^2 f}{\partial \boldsymbol{R}^2}\right|_{\boldsymbol{R}=\boldsymbol{r}} \tag{58}$$

When the approximation expressed by Eq. (56) is applied to Eqs. (8) and (9), and higher-order terms are neglected, the explicit forms of forces and torques are derived by Eqs. (60) and (61). Here, the moment of inertia tensor is defined by the equation below.

$$\boldsymbol{I}=\int(|\boldsymbol{\rho}|^2\boldsymbol{E}-\boldsymbol{\rho}\boldsymbol{\rho}^{\mathrm{T}})dm \tag{59}$$

$$\begin{aligned}
\boldsymbol{F}_{G,C_{00}} &= -\frac{m\mu}{|\boldsymbol{r}|^3}\boldsymbol{r} \\
\boldsymbol{F}_{G,coup} &= -\frac{3\mu}{|\boldsymbol{r}|^5}\boldsymbol{I}\boldsymbol{r}-\frac{3}{2}\frac{\mu}{|\boldsymbol{r}|^5}\mathrm{tr}(\boldsymbol{I})\boldsymbol{r}+\frac{15}{2}\frac{\mu}{|\boldsymbol{r}|^7}(\boldsymbol{r}^{\mathrm{T}}\boldsymbol{I}\boldsymbol{r})\boldsymbol{r} \\
\boldsymbol{F}_{G,C_{2k}} &= m\mu C_{20}R_a^2\left(-\frac{15}{2}\frac{(\boldsymbol{\gamma}\cdot\boldsymbol{r})^2}{|\boldsymbol{r}|^7}\boldsymbol{r}+3\frac{\boldsymbol{\gamma}\cdot\boldsymbol{r}}{|\boldsymbol{r}|^5}\boldsymbol{\gamma}+\frac{3}{2}\frac{1}{|\boldsymbol{r}|^5}\boldsymbol{r}\right) \\
&\quad +m\mu C_{22}R_a^2\left(-15\frac{(\boldsymbol{\alpha}\cdot\boldsymbol{r})^2-(\boldsymbol{\beta}\cdot\boldsymbol{r})^2}{|\boldsymbol{r}|^7}\boldsymbol{r}+6\frac{\boldsymbol{\alpha}\cdot\boldsymbol{r}}{|\boldsymbol{r}|^5}\boldsymbol{\alpha}-6\frac{\boldsymbol{\beta}\cdot\boldsymbol{r}}{|\boldsymbol{r}|^5}\boldsymbol{\beta}\right) \\
\boldsymbol{F}_{G,C_{4k}} &= m\mu C_{40}R_a^4\left(-\frac{315}{8}\frac{(\boldsymbol{\gamma}\cdot\boldsymbol{r})^4}{|\boldsymbol{r}|^{11}}\boldsymbol{r}+\frac{35}{2}\frac{(\boldsymbol{\gamma}\cdot\boldsymbol{r})^3}{|\boldsymbol{r}|^9}\boldsymbol{\gamma}+\frac{105}{4}\frac{(\boldsymbol{\gamma}\cdot\boldsymbol{r})^2}{|\boldsymbol{r}|^9}\boldsymbol{r}-\frac{15}{2}\frac{\boldsymbol{\gamma}\cdot\boldsymbol{r}}{|\boldsymbol{r}|^7}\boldsymbol{\gamma}-\frac{15}{8}\frac{1}{|\boldsymbol{r}|^7}\boldsymbol{r}\right) \\
&\quad +m\mu C_{42}R_a^4\left(-\frac{945}{2}\frac{\{(\boldsymbol{\alpha}\cdot\boldsymbol{r})^2-(\boldsymbol{\beta}\cdot\boldsymbol{r})^2\}(\boldsymbol{\gamma}\cdot\boldsymbol{r})^2}{|\boldsymbol{r}|^{11}}\boldsymbol{r}+105\frac{(\boldsymbol{\alpha}\cdot\boldsymbol{r})(\boldsymbol{\gamma}\cdot\boldsymbol{r})^2}{|\boldsymbol{r}|^9}\boldsymbol{\alpha}\right. \\
&\qquad -105\frac{(\boldsymbol{\beta}\cdot\boldsymbol{r})(\boldsymbol{\gamma}\cdot\boldsymbol{r})^2}{|\boldsymbol{r}|^9}\boldsymbol{\beta}+105\frac{\{(\boldsymbol{\alpha}\cdot\boldsymbol{r})^2-(\boldsymbol{\beta}\cdot\boldsymbol{r})^2\}(\boldsymbol{\gamma}\cdot\boldsymbol{r})}{|\boldsymbol{r}|^9}\boldsymbol{\gamma} \\
&\qquad \left.+\frac{105}{2}\frac{(\boldsymbol{\alpha}\cdot\boldsymbol{r})^2-(\boldsymbol{\beta}\cdot\boldsymbol{r})^2}{|\boldsymbol{r}|^9}\boldsymbol{r}-15\frac{\boldsymbol{\alpha}\cdot\boldsymbol{r}}{|\boldsymbol{r}|^7}\boldsymbol{\alpha}+15\frac{\boldsymbol{\beta}\cdot\boldsymbol{r}}{|\boldsymbol{r}|^7}\boldsymbol{\beta}\right) \\
&\quad +m\mu C_{44}R_a^4\left(-945\frac{(\boldsymbol{\alpha}\cdot\boldsymbol{r})^4+(\boldsymbol{\beta}\cdot\boldsymbol{r})^4-6(\boldsymbol{\alpha}\cdot\boldsymbol{r})^2(\boldsymbol{\beta}\cdot\boldsymbol{r})^2}{|\boldsymbol{r}|^{11}}\boldsymbol{r}+420\frac{(\boldsymbol{\alpha}\cdot\boldsymbol{r})^3}{|\boldsymbol{r}|^9}\boldsymbol{\alpha}\right. \\
&\qquad \left.+420\frac{(\boldsymbol{\beta}\cdot\boldsymbol{r})^3}{|\boldsymbol{r}|^9}\boldsymbol{\beta}-1260\frac{(\boldsymbol{\alpha}\cdot\boldsymbol{r})(\boldsymbol{\beta}\cdot\boldsymbol{r})^2}{|\boldsymbol{r}|^9}\boldsymbol{\alpha}-1260\frac{(\boldsymbol{\alpha}\cdot\boldsymbol{r})^2(\boldsymbol{\beta}\cdot\boldsymbol{r})}{|\boldsymbol{r}|^9}\boldsymbol{\beta}\right)
\end{aligned} \tag{60}$$

$$\begin{aligned}
\boldsymbol{T}_{GG,C_{00}} &= -\frac{3\mu}{|\boldsymbol{r}|^5}\boldsymbol{r}\times\boldsymbol{I}\boldsymbol{r} \\
\boldsymbol{T}_{GG,C_{2k}} &= \mu C_{20}R_a^2\left\{\left(\frac{105}{2}\frac{(\boldsymbol{\gamma}\cdot\boldsymbol{r})^2}{|\boldsymbol{r}|^9}-\frac{15}{2}\frac{1}{|\boldsymbol{r}|^7}\right)\boldsymbol{r}\times\boldsymbol{I}\boldsymbol{r}-15\frac{\boldsymbol{\gamma}\cdot\boldsymbol{r}}{|\boldsymbol{r}|^7}(\boldsymbol{r}\times\boldsymbol{I}\boldsymbol{\gamma}+\boldsymbol{\gamma}\times\boldsymbol{I}\boldsymbol{r})+3\frac{1}{|\boldsymbol{r}|^5}\boldsymbol{\gamma}\times\boldsymbol{I}\boldsymbol{\gamma}\right\} \\
&\quad +\mu C_{22}R_a^2\left(105\frac{(\boldsymbol{\alpha}\cdot\boldsymbol{r})^2-(\boldsymbol{\beta}\cdot\boldsymbol{r})^2}{|\boldsymbol{r}|^9}\boldsymbol{r}\times\boldsymbol{I}\boldsymbol{r}-30\frac{\boldsymbol{\alpha}\cdot\boldsymbol{r}}{|\boldsymbol{r}|^7}(\boldsymbol{r}\times\boldsymbol{I}\boldsymbol{\alpha}+\boldsymbol{\alpha}\times\boldsymbol{I}\boldsymbol{r})\right. \\
&\qquad \left.+30\frac{\boldsymbol{\beta}\cdot\boldsymbol{r}}{|\boldsymbol{r}|^7}(\boldsymbol{r}\times\boldsymbol{I}\boldsymbol{\beta}+\boldsymbol{\beta}\times\boldsymbol{I}\boldsymbol{r})+6\frac{1}{|\boldsymbol{r}|^5}(\boldsymbol{\alpha}\times\boldsymbol{I}\boldsymbol{\alpha}-\boldsymbol{\beta}\times\boldsymbol{I}\boldsymbol{\beta})\right\}
\end{aligned} \tag{61}$$

References

1. D. J. Scheeres, "Satellite Dynamics about Asteroids," *Advances in the Astronautical Sciences*, Vol. 87, 1994, pp. 275–292.
2. D. J. Scheeres, S. J. Ostro, R. S. Hudson, E. M. Dejong, and S. Suzuki, "Dynamics of Orbits

Close to Asteroid 4179 Toutatis," *Icarus*, Vol. 132, 1998, pp. 53–79.

3. D. J. Scheeres, "Satellite Dynamics about Small Bodies: Averaged Solar Radiation Pressure Effects," *Journal of the Astronautical Sciences*, Vol. 47, No.1, 1999, pp.25–46.
4. H. D. Curtis, *Orbital Mechanics for Engineering Students*, Elsevier, Burlington, MA, 2005.
5. D. Lantukh, R. P. Russell, and S. Broschart, "Heliotropic Orbits at Oblate Asteroids: Balancing Solar Pressure and J2 Perturbations," *Celestial Mechanics and Dynamical Astronomy*, Vol. 121, 2015, pp. 171–190.
6. J. Riverin, and A. K. Misra, "Attitude Dynamics of Satellites Orbiting Small Bodies," *AIAA/AAS Astrodynamics Specialist Conference and Exhibit*, Monterey, CA, 2002.
7. Y. Wang, S. Xu, "Gravity Gradient Torque of Spacecraft Orbiting Asteroids," *Aircraft Engineering and Aerospace Technology*, Vol. 85, No. 1, 2013, pp. 72–81.
8. Y. Wang, S. Xu, "Attitude Stability of a Spacecraft on a Stationary Orbit around an Asteroid Subjected to Gravity Gradient Torque," *Celestial Mechanics and Dynamical Astronomy*, Vol. 115, No. 4, 2013, pp. 333–352.
9. J. R. Wertz, *Spacecraft Attitude Determination and Control*, Kluwer Academic, Boston, 1978.
10. G. B. Sincarsin, P. C. Hughes, "Gravitational Orbit-Attitude Coupling for Very Large Spacecraft," *Celestial Mechanics*, Vol. 31, No. 2, 1983, pp. 143–161.
11. B. Wong, R. Patil, and A. Misra, "Attitude Dynamics of Rigid Bodies in the Vicinity of Lagrangian Points," Vol. 31, No. 1, 2008, pp 252–256.
12. A. Knutson and K. C. Howell, "Coupled Orbit and Attitude Dynamics for Spacecraft Composed of Multiple Bodies in Earth-Moon Halo Orbits", *63rd International Astronautical Congress*, Naples, Italy, 2012.
13. D. Guzzetti and K. C. Howell, "Natural Periodic Orbit-Attitude Behaviors for Rigid Bodies in Three-Body Periodic Orbits," *Acta Astronautica*, 2016.
14. Y. Wang, and S. Xu, "Gravitational Orbit-Rotation Coupling of a Rigid Satellite around a Spheroid Planet," *Journal of Aerospace Engineering*, Vol. 27, No. 1, 2014, pp. 140–150.
15. Y. Wang, S. Xu, and M. Zhu, "Stability of Relative Equilibria of the Full Spacecraft Dynamics around an Asteroid with Orbit-Attitude Coupling," *Advances in Space Research*, Vol. 53, No. 7, 2014, pp. 1092–1107.
16. G. Misra, M. Izadi, A. Sanyal, and D. J. Scheeres, "Coupled Orbit-Attitude Dynamics and Relative State Estimation of Spacecraft Near Small Solar System Bodies," *Advances in Space Research*, Vol. 57, No. 8, 2016, pp. 1747–1761.
17. J. Kawaguchi, T. Kominato, and K. Shirakawa, "Attitude Control Flight Experience: Coping with Solar Radiation and Ion Engines Leak Thrust in Hayabusa (MUSES-C)," *20th International Symposium on Space Flight Dynamics*, Annapolis, MD, 2007.
18. G. Ono, Y. Tsuda, K. Akatsuka, T. Saiki, Y. Mimasu, N. Ogawa, and F. Terui, "Generalized Attitude Model for Momentum-Biased Solar Sail Spacecraft," *Journal of Guidance, Control, and Dynamics*, 2016.
19. Y. Tsuda, M. Yoshikawa, M. Abe, H. Minamino, and S. Nakazawa, "System Design of the Hayabusa 2—Asteroid Sample Return Mission to 1999 JU3," *Acta Astronautica*, Vol. 91, 2013, pp. 356–362.
20. A. Kryszczyńska, A. La Spina, P. Paolicchi, A. W. Harris, S. Breiter, and P. Pravec, "New Findings on Asteroid Spin-Vector Distributions," *Icarus*, Vol. 192, No. 1, 2007, pp. 223–237.
21. D. J. Scheeres, B. G. Williams, W. E. Bollman, R. P. Davis, C. E. Helfrich, S. P. Synnott, and D. K. Yeomans, "Navigation for Low-Cost Missions to Small Solar-System Bodies," *Acta Astronautica*, Vol. 35, 1995, pp. 211–220.
22. C. R. Mclnnes, *Solar Sailing: Technology, Dynamics and Mission Applications*, Springer Praxis, Chichester, 1999.
23. D. J. Scheeres, *Orbital Motion in Strongly Perturbed Environments*, Springer Praxis, 2012.
24. A. Rossi, F. Marzari, and P. Farinella, "Orbital Evolution around Irregular Bodies," *Earth, planets and space*, Vol. 51, No. 11, 1999, pp. 1173–1180.
25. D. J. Scheeres, "Spacecraft Dynamics in the Vicinity of a Comet," *Journal of the Astronautical Sciences*, Vol. 50, No.1, 2002, pp. 35–52.
26. J. Laskar, "Frequency Map Analysis of an Hamiltonian System," *American Institute of Physics Conference Proceedings*, Vol. 344, 1995, pp. 130–159.
27. N. Bosanac, K. C. Howell, and E. Fischbach, "Exploring the Impact of a Three-Body Interaction Added to the Gravitational Potential Function in the Restricted Three-Body Problem," *23rd AAS/AIAA Space Flight Mechanics Meeting*, Kauai, HI, 2013.